Influence of β on the self-similarity properties of LHD edge fluctuations

D Carralero[1], I Calvo[1], M Shoji[2], B A Carreras[3], K Ida[2], S Ohdachi[2], S Sakakibara[2], H Yamada[2] and C Hidalgo[1]

[1] Laboratorio Nacional de Fusión, Asociación EURATOM-CIEMAT, 28040 Madrid, Spain

[2] National Institute for Fusion Science, 322-6 Oroshi-cho, Toki 509-5092, Japan

[3] BACV Solutions Inc., Oak Ridge, TN 37830, U.S.A.

E-mail: daniel.carralero@ciemat.es

Abstract. The parameter $\langle\beta\rangle$, measuring confinement efficiency, is one of the main figures of merit of a magnetic fusion device. Present-day limits to its increase are not imposed by disruptive MHD activity but rather by edge confinement degradation. Large Helical Device heliotron has recently achieved record $\langle\beta\rangle$ values up to 5%. At the same time, recent fast camera experiments have revealed that this operational regime is characterized by the stochastic ejection of macroscopic structures in the form of filaments. In this work we apply suitable statistical tools to the analysis of the ejection sequence of such structures, as measured by the camera, and show that it possesses a self-similar, persistent character. Some self-similar properties of the stochastic process (namely the Hurst parameter and the waiting-time distribution) are studied and found to be dependent on the value of $\langle\beta\rangle$. These experimental results are interpreted in the light of previous theoretical works and the existence of self-organization is discussed.

PACS numbers: 52.55.-s 05.65.+b 52.35.Ra 89.75.Fb

1. Introduction

The volume-averaged beta parameter $\langle\beta\rangle$ of a magnetic confinement device, where $\beta = 2\mu_0 p/B^2$ (i.e. the ratio of the plasma and the magnetic pressure), can be regarded as a measure of the overall efficiency of the system as it determines, for a given plasma density and temperature, the magnitude of the magnetic field and thus the size, complexity and cost of the coil system. Therefore, the achievement of high $\langle\beta\rangle$ values both in present-day and next generation machines such as ITER is of paramount importance for the technological and economic viability of future nuclear fusion reactors. Currently, the record $\langle\beta\rangle$-value in a reactor-relevant device is held by the Large Helical Device (LHD) heliotron with $\langle\beta\rangle = 5\%$ sustained up to ten times the confinement time. Traditionally, the increase of $\langle\beta\rangle$ was limited by the onset of disruptive MHD instabilities (ballooning, ideal or resistive interchange instabilities) [1], but after recent developments, last LHD record $\langle\beta\rangle$ values have been reached without giving rise to strong MHD activity: by a careful selection of an inwards shifted magnetic configuration NBI heating is improved, Shafranov shift effect limited and MHD activity either reduced or kept stable [2, 3, 4]. Up to now, MHD stability has proved not to be a limiting factor in this configuration, with no global disruptions taking place as $\langle\beta\rangle$ increases [4, 5]. Nevertheless, experimental data show a degradation of confinement caused by enhanced thermal transport in the periphery when $\langle\beta\rangle \simeq 3\%$ is surpassed [6], usually displaying a flattening of the T_e profile. A natural candidate to explain this is turbulence-driven transport which, since the 80s, has been considered (in the absence of macroscopic instabilities) the predominant mechanism for particle and heat outflux. Indeed, turbulence has already been proposed as an explanation for these phenomena in Ref. [7].

Recent experiments [8] carried out in LHD provide further evidence favoring the turbulence-induced transport hypothesis: a series of systematic fast camera observations revealed, as an exclusive feature of high-β discharges, the ejection of macroscopic filament-like structures from the limit of the ergodic layer into the Scrape-Off Layer (SOL). In Ref. [8], the geometry and experimental interpretation of camera signals are explained and the filaments are identified as macroscopic plasma density fluctuations traveling radially outwards. Additionally, an inspection of the filament ejection frequency spectra showed that a fraction of the spectral power was distributed in a coherent mode (around 3 kHz), and there was also a wide region of the spectrum (from 4 to 10 kHz) displaying uncoherent stochastic activity. The first one could be clearly related to an $m/n = 2/3$ edge mode by comparison with magnetic probe data. By means of frequency filters, it was determined that the filament-like structures belonged to the second one, which remained to be investigated and is the subject of the present work. The irregular, self-similar expulsion of well-differentiated structures of varying sizes into the ergodic layer is reminiscent of situations where plasma self-organization gives rise to avalanches and non-diffusive transport [9, 10, 11]. Such non-diffusive plasmas display a number of distinct properties like long-term memory effects (non-markovianity). The

main objective of the present work is to measure these properties of edge turbulence and their evolution with $\langle\beta\rangle$, and for that an appropriate statistical analysis of the camera data is carried out. Thomson Scattering pressure-profile data will also be provided as complementary information. Additionally, the possible role of self-organization, which has been specifically proposed in LHD high-β plasmas [5] as a mechanism to stabilize the pressure profile against MHD instabilities, will be discussed in connection with theoretical works.

The rest of the paper is organized as follows. In Section 2 the experimental layout and signal interpretation are outlined. Some insight about data selection criteria is also provided. In Section 3 the rescaled-range and waiting-times statistical analysis techniques are explained and the results of the experimental data analysis are shown. In Section 4 those results are discussed and some bibliography is reviewed. Finally, conclusions are summarized in Section 5.

2. Experimental Layout and Data

The experimental layout employed is extensively explained in [8]: a Photron APX-RS fast camera was coupled to a 75 mm objective by a 4.5 m long coherent optical fibers bundle in order to protect it from the intense magnetic fields of LHD. As shown in Fig. 1 (left), the objective was placed on LHD 6-T tangential port, overlooking a region of almost 90° of the vacuum vessel. Pixel resolution varies with the sampling rate, ranging from 1024x1024 pixels up to 5 kHz to 192x136 pixels for 50 kHz. Of course, the actual resolution (in spatial units per pixel) depends on the distance of the observation region to the camera. In the divertor leg region analyzed in this paper, 1 pixel corresponds to some 5 mm. Visible radiation detected by the camera is produced by line radiation of light elements (essentially H_α and Carbon II), which takes place in relatively cold regions of the plasma, like the edge. Typical SOL is usually under the so called "ionizing plasma edge conditions" (T_e under 100eV, n_e 10^{19} m^{-3} near the Last Closed Flux Surface). In such conditions, the excitation rate is essentially constant and the signal can be regarded as proportional to n_e and n_o in the point of emission, where n_o is the emitting element neutrals density. In Fig. 1 (right), a general view of a typical high-β discharge is displayed. A Poincaré plot of the vacuum magnetic field corresponding to the vertical plane defined by the blue line on the equatorial view on the left is superimposed. The photograph shows two bright curves corresponding to the two main emission areas: the strike point of the divertor leg in the vacuum vessel wall and the X-point region in the outer ergodic layer. Note that although there seems to be a gap between the position of the ergodic layer and the X-point emission region, the plasma is shifted radially outwards due to the Shafranov shift and, according to HINT finite β simulations [2], the shift (15 cm) is such that both regions roughly coincide. Between the X and strike points, the divertor leg appears as a slightly illuminated area. Finally, the 192x136 pixels reduced area for 50 kHz sampling is displayed as a darkened rectangle.

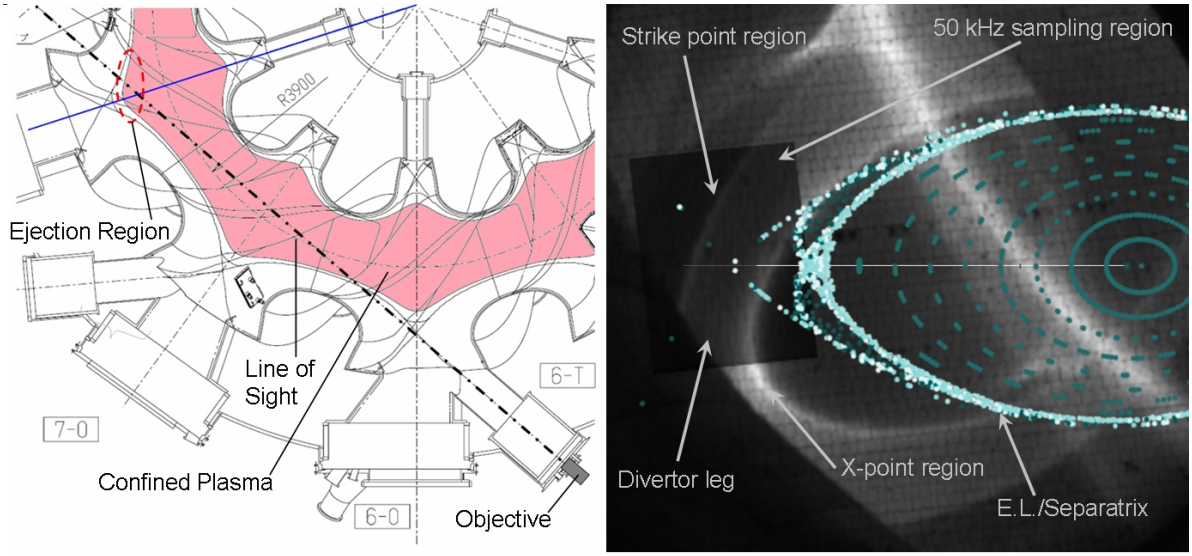

Figure 1. (color online). Experimental layout. (Left) top view of LHD equatorial section. Camera objective at 6T port and its line of sight are displayed. The region where filaments are observed is marked in red. (Right) General view of a typical high-β plasma. X and strike point regions appear as bright curves, with the divertor leg stretching in between. A Poincar map of the vacuum field at the vertical plane defined as a blue line on the left is superposed. Dark blue curves represent closed surfaces while bright ones represent the ergodic layer/separatrix. The limited region observed at 50 kHz sampling rate appears as a darkened rectangle.

As shown in previous work, when high-β optimized configuration plasmas ($R_{axis} =$ 3.6 m, $B_q = 100\%$, $\gamma = 1.197$) are produced, fast propagating structures appear on the divertor leg, being ejected from the X-point and propagating towards the wall. Fig. 2 (top) displays a typical ejection event as observed by the camera: when only the fluctuation of the signal is displayed, it is possible to see how an elongated structure is formed in the X-point region and then released into the divertor leg. These events are quite fast and 50 kHz operation is required to distinguish individual filaments. If the raw data collected in a single pixel near the ejection area (indicated as a red cross) during a long interval is displayed (figure 2, bottom left), a number of such ejection events can be identified even by the naked eye. This density fluctuation signal can be considered a good measure of the size and duration of the ejected structures, in the range of several cm and some 100 μs, respectively. Although it is not a direct measure of the radial flux, it is related to the latter since it was found in previous work that the kind of macroscopic structures measured by the camera in the ergodic layer region always propagate radially outwards at similar velocities (in the range of 3-5 km/s) in this regime.

To carry out the proposed analysis, a careful observation of high β plasmas was performed: during two LHD experimental campaigns several hundred discharges with high-β optimized magnetic configuration were recorded at a 50 kHz frame rate. From

these movies, a density fluctuation evolution signal was obtained from several points on the external edge of the ergodic layer, in the vicinity of the X-point of the horizontally elongated section highlighted in Fig. 1. Long-term correlation analysis require correspondingly long and stationary signals. Therefore, from the original set of measured discharges, a selection was made in order to choose only those displaying long periods (of at least 150 ms) of stable conditions (density, $\langle\beta\rangle$, NBI injection, etc.). After the selection, some dozen interesting intervals remained, covering a wide range of $\langle\beta\rangle$ regimes (from 1.8% to 4.5%). Finally, comparing the selected discharge data, one sampling point is selected in each one to generate a single series. When doing so, a compromise between saturation due to X-point glow and fading of the filament signal was achieved. In all cases, the selected point position with respect to the ergodic layer is equivalent (and roughly equal to that highlighted in the first frame of Fig. 2 (top).

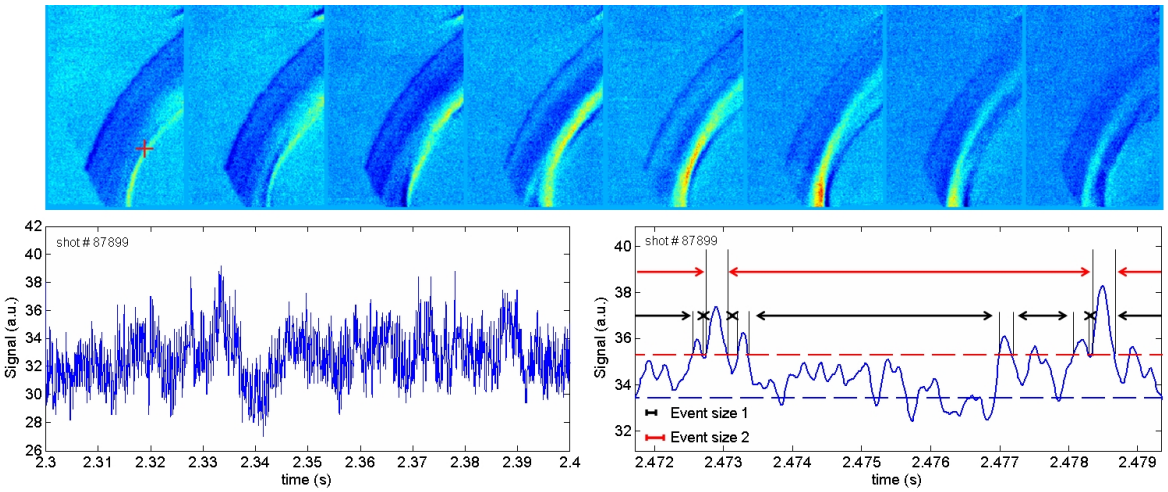

Figure 2. (color online). (Top) Typical filament ejection sequence recorded at 50 kHz in the darkened region of Fig. 1. Only the fluctuating part of the signal is displayed. (Bottom,left) Raw data measured in a single pixel near the X-point (position marked as a red cross in top sequence) during a 100 ms interval. (Bottom, right) Waiting time selection process for two event sizes on the same raw data: mean value and value threshold (mean plus 1.5 times the standard deviation) are displayed as blue and red dashed lines respectively. Events are defined as times when the signal exceeds the value threshold. Waiting times (colored arrows) are defined as intervals between events which are equal or greater than the selected minimum event size.

3. Statistical Analysis of Results

Once a number of time series of fluctuations were selected over a range of $\langle\beta\rangle$ values, a statistical analysis of the filament ejection activity was carried out. As announced in the Introduction, the main objective of this paper is to detect traces of long-term correlations and non-markovianity in the statistical behavior of the filament ejection

pattern. Firstly, the scaling with time of the square root of the second-moment of the signal, the so called *Hurst parameter* H, was determined. A robust way to compute H is to use the rescaled range or R/S technique [12]. Given a discrete time series $\{X_n\}$ we define

$$[R/S](\tau) := \frac{\max_{1\leq k\leq\tau}\{W_k\} - \min_{1\leq k\leq\tau}\{W_k\}}{\sqrt{\langle X^2\rangle_\tau - \langle X\rangle_\tau^2}},$$

$$W_k := X_1 + X_2 + ... + X_k - k\langle X\rangle_\tau,$$

where $\langle X\rangle_k$ is the average of X over the $[1, k]$ interval. For a self-similar series, $[R/S](\tau) \propto \tau^H$. Whereas $H = 1/2$ indicates that the series entries are not correlated (typically associated to diffusive transport phenomena), $H > 1/2$ corresponds to positively correlated entries (superdiffusion), and $H < 1/2$ to negatively correlated entries (subdiffusion). Of course, the algebraic behavior $[R/S](\tau) \propto \tau^H$ should not be expected at all scales but only at those where the signal is actually self-similar [13]. This analysis has been applied to edge fluctuations in several tokamaks (JET, TJ-I, DIII-D, MAST, TEXTOR) and stellarators (W7-AS, TJ-IU, ATF) [14, 15, 16], obtaining moderately persistent H values (i.e., greater than 1/2) in the range of 0.6-0.7. It must be noted that all these previous experiments were carried out in a range of the β parameter well under the one explored in the present work ($\langle\beta\rangle < 2\%$ in all cases).

A representative result of the R/S analysis in LHD high β plasmas can be seen in Fig. 3 where indeed three different regions appear. Region I, ranging up to several hundreds of μs, has $H \simeq 1$. However, this time scale corresponds to the duration of single events and its ballistic behavior is rather trivial [13]. Between regions I and II an elbow is found (red circle), followed by a flatter region. This time corresponds to the period of the m/n=2/3 mode activity (which can also be seen in the spectrum of the signal [8]) and the elbow is the characteristic signature of a coherent mode in $[R/S](\tau)$ [14]. Region II is the relevant one, the self-similar range exhibiting the non-trivial correlation between fluctuations at different times. In this region, which lasts around a decade, we find $H = 0.94$, which reveals strong persistence for large time lag in the time series analyzed. To ensure this, an illuminating test [13] is performed: the whole signal is divided in segments of the size of the events (200 μs) and then those segments are randomly shuffled. As expected, $[R/S](\tau)$ for the shuffled time series (green curve in Fig. 3) is identical to the original one in Region I but loses the persistent behavior in Region II, where H acquires a value close to 1/2. This shows that the Hurst exponent found for the original time series in Region II is non-trivially generated by the dynamics and consistent with the SOC interpretation. Region III possesses $H \simeq 1/2$, probably due to finite-size effects in the time series [13] (the time scale is over the confinement time). Still, this region represents intervals with lengths close to that of the data series and the reliability of the R/S method is thus decreased in it. Therefore, no further analysis will be carried out for this last region. The same analysis is repeated for discharges with several $\langle\beta\rangle$ values.

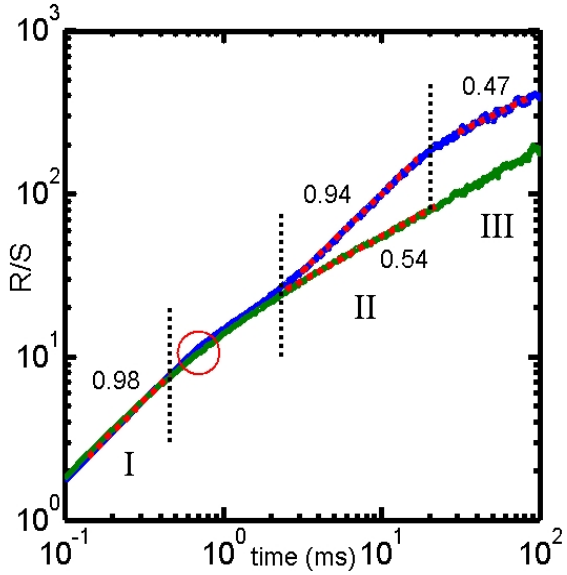

Figure 3. (color online). Typical result of an R/S analysis: the blue curve corresponds to the analyzed time series and the green curve displays the result of the shuffling test. The different values of the Hurst exponent in each region are given. The red circle indicates the elbow between regions I and II.

In Fig. 4, the value of H in Region II (i.e. the relevant time scale) as a function of $\langle\beta\rangle$ is plotted. For $\langle\beta\rangle < 2\%$ one obtains the aforementioned usual values of H reported in the literature (shaded region). Then, H increases with $\langle\beta\rangle$, reaches a maximum at $\langle\beta\rangle \approx 3\% - 3.5\%$ and decreases to the initial values for $\langle\beta\rangle \simeq 4.5\%$. Again, to ensure the validity of the results, shuffling tests are performed, getting $H \approx 1/2$ for the shuffled time series at every value of $\langle\beta\rangle$, as expected. We would like to stress that several data points correspond to the same discharge at two different $\langle\beta\rangle$ regimes (see figure caption). The computation of H in two different $\langle\beta\rangle$ regimes within the same discharge increases the reliability of the results, discarding effects of eventual uncontrolled variations of parameters other than $\langle\beta\rangle$.

As a complementary analysis aimed to give a further check of the non-markovianity found by the R/S calculation, the *waiting-time* probability distribution function (pdf), i.e. the pdf of the time elapsed between two consecutive events, was studied. The process for the calculation of those pdfs is summarized in Fig. 2 (bottom, right). In it, raw data sequences (like the one in Fig. 2 bottom left) are considered. First, a threshold value is defined (1.5 times the standard deviation in our case). Then, those parts of the signal over the threshold are called *events*. Last, an event size is defined and the time elapsed between two events with a duration exceeding that event size is called a *waiting time*. Like this, several pdfs of all waiting times are obtained, filtering the events by their size: only events over a certain duration are considered and those under that duration are ignored when defining the waiting times, which become longer

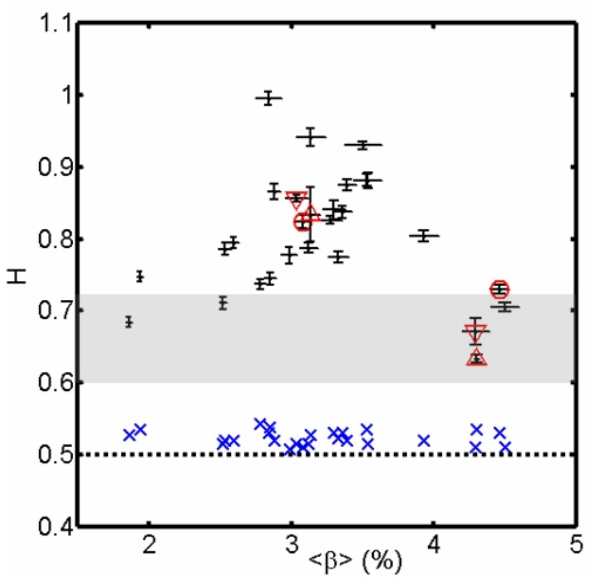

Figure 4. (color online). Value of H in Region II (as defined in Fig. 3) for several $\langle\beta\rangle$ regimes. The shaded area corresponds to the usual H-values reported in the literature. Points with the same red symbol correspond to the same discharge. The values of H for the shuffled time series are represented by blue crosses.

and fewer than before filtering. These distributions are closely related to the presence of long-term correlations: according to Ref. [17], where a more detailed explanation about this method can be found, the waiting-time pdf ("quiet times" in the language of Ref. [17]) of large events decays as a power law when long-term correlations are present.

The waiting-time analysis of our experimental data is shown in Fig. 5. For a number of selected representative discharges covering the $\langle\beta\rangle$ range, the waiting-time pdf as a function of the filtering value (the duration, or "size" of the event) is shown. In all cases, it can be seen how the distribution including all events shows an approximately exponential decay (except for very long waiting-times). When the events with the shortest duration are filtered out, the variation of the waiting-time pdf depends on $\langle\beta\rangle$: whereas the low $\langle\beta\rangle$ case shows hardly any difference, the $\langle\beta\rangle = 3 - 3.5\%$ discharges show a clear power law which lasts more than one decade. As $\langle\beta\rangle$ increases, the length of this power law region decreases, although no return to the exponential-like behavior can be observed. Consistently with R/S analysis, long-term correlations, encoded here in the fat tail of the waiting-time pdf, are stronger for those $\langle\beta\rangle$-values in which H is maximum.

Last, electron pressure profiles have been measured during the analyzed intervals by means of a Thomson scatering system. Pressure profiles are time-averaged over the interval in which H is calculated and normalized with B^2 (B is the toroidal magnetic field at the axis), thus allowing the comparison between discharges with different magnetic field In Fig. 6, several porfiles are displayed for a number of different $\langle\beta\rangle$ values.

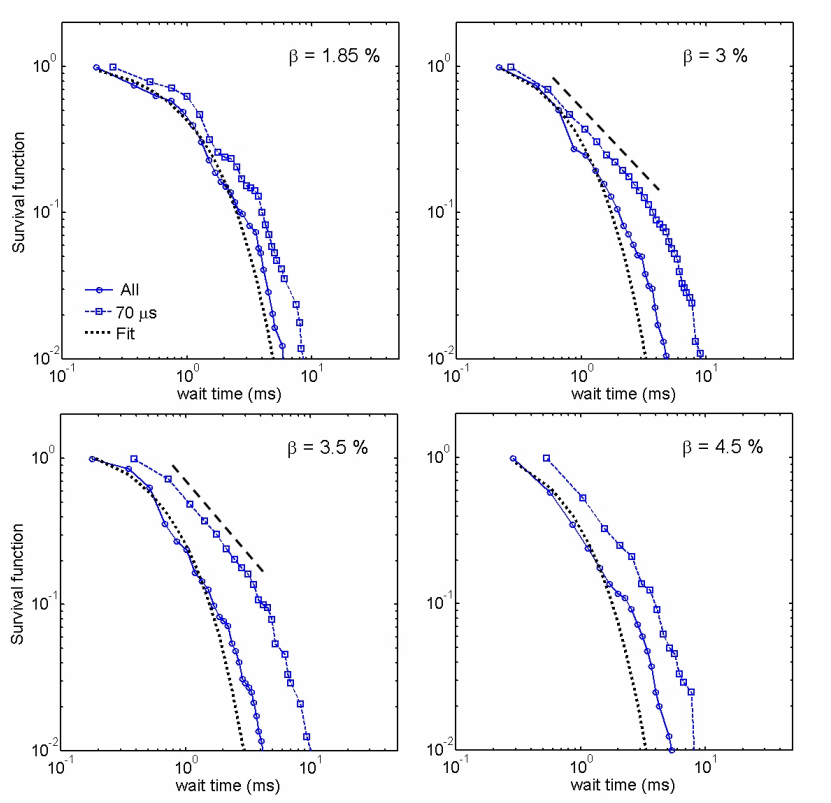

Figure 5. (color online). Waiting-time pdf for several values of $\langle\beta\rangle$ and computed with and without threshold in the event-size. The black dotted line is the exponential fit for the pdf including all events. Algebraic regions are highlighted where appropriate with a black dashed line.

4. Discussion

The essential results of this paper are contained in Figs. 3, 4, and 5. Fast camera experimental data reveal self-similar behavior in the ejection of macroscopic structures for high-β LHD discharges: the Hurst parameter, which gives a measure of the long term-correlation of the fluctuations, is clearly related to $\langle\beta\rangle$ and reaches its largest (strongly persistent) values for $\langle\beta\rangle \approx 3-4\%$. In this range of $\langle\beta\rangle$, the distribution function of waiting times between ejection events develops an algebraic tail when only large events (with a duration of more than 70-90 μs) are considered. We would like to emphasize that the time scale in which the R/S analysis shows a non-trivial self-similar behavior coincides with that of the typical interval between large events (1-10 ms), and with the region in which the waiting-time pdf becomes algebraic. These statistical properties seem to suggest that the increase of $\langle\beta\rangle$ introduces a change in the nature of the transport, which might become superdiffusive over a range of values.

The stochastic ejection of macroscopic structures and the results obtained in Section 3 from the statistical analysis of the ejection pattern (superdiffusive character and alge-

braic waiting-time pdfs for large events) suggest that Self-Organized Criticality (SOC) dynamics might be involved. The paradigm of SOC was introduced in Ref. [18] and many natural phenomena have been interpreted in terms of it (see, for example, Refs. [19] or [20]). In the field of turbulent fusion plasmas, a translation of these ideas was realized in Ref. [9], [21], or [22] and [23], where the SOC ingredients were identified in a resistive pressure-gradient-driven turbulence model. Also, it was shown that particle tracer transport in the model studied in Ref. [23] is superdiffusive. Moreover, in Ref. [10] SOC, superdiffusive transport and confinement degradation in turbulent fusion plasmas were linked. Besides, a positive effect of SOC has been reported in Ref. [5], where self-organization of pressure profiles is specifically proposed as the mechanism that allows LHD to reach high $\langle\beta\rangle$ values by non-linearly stabilizing linearly unstable low-n ideal interchange modes.

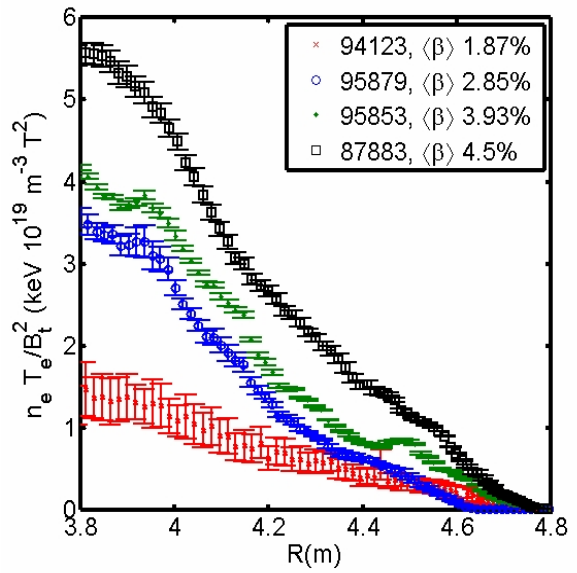

Figure 6. (color online). Normalized electron pressure evolution with $\langle\beta\rangle$. Given the robustness of the pressure profile, $\langle\beta\rangle$ provides a good measure of the local value of β and its gradient in the region where the instability is originated.

In order to substantiate our interpretation we resort to comparison with the theoretical work on plasma turbulence from the SOC perspective performed in Ref. [23]. Therein, the drive of the system is, essentially, the parameter β, and the critical condition is a threshold in the local pressure gradient. It turns out that in the SOC state the pressure profile is stagnant. Moreover, theoretical models predict that the system can remain in this critical state as the drive is increased until it is so large that the profile can not be relaxed anymore. At that point, the system becomes supercritical and SOC dynamics disappears. Next, the relationship between $\langle\beta\rangle$ and the experimental LHD edge electron pressure profiles is studied. Gradients are considered in the region $R = 4.2 - 4.8$ m (see Fig. 6), corresponding to the plasma edge and ergodic layer. The

analysis reveals remarkable similarities to the expected behavior; indeed, as Fig. 6 shows, the pressure gradient increases with $\langle\beta\rangle$, becomes almost stagnant around $\langle\beta\rangle = 3\%$, and grows rapidly again for the highest $\langle\beta\rangle$-values. Finally, according to Ref. [10], the expected implications of SOC emergence on LHD overall performance would be a degradation of confinement and an increase of the power necessary to keep β growing beyond that point. Both effects are reported in the literature: in [24], where confinement is analyzed for high-β discharges, the confinement time, τ_E, falls under the ISS95 scaling for $\langle\beta\rangle \approx 3\%$ and the $\langle\beta\rangle$ dependence of the absorbed power changes from $\langle\beta\rangle \propto P_{abs}^{0.4}$ to $\langle\beta\rangle \propto P_{abs}^{0.25}$ around the same value. A word of caution is in order: a recovery in the scaling does not need to take place when the SOC regime is surpassed; on the contrary, it is expected that when SOC is overran (and therefore H decreases) the level of fluctuations, and with it radial transport, is increased.

5. Conclusions

To summarize, elongated, filament-like structures are observed by fast camera imaging during high-β configuration LHD discharges. These structures are ejected from the ergodic layer into the SOL, in an apparently stochastic sequence. Fast camera data reveal that ejection of macroscopic structures has non-markovian statistical properties, namely long-term correlations. Furthermore, both R/S and waiting time analysis show how those properties are clearly related to $\langle\beta\rangle$, reaching a maximum for $\langle\beta\rangle \approx 3-3.5\%$. These results seem to suggest a dependence on $\langle\beta\rangle$ of the nature of the transport, which would become increasingly non-markovian (and therefore non-diffusive) as $\langle\beta\rangle$ increases, until the maximum is reached and the Hurst parameter drops again. One possible interpretation of this might be some form of turbulence self-organization, such as SOC. This mechanism, although speculative, would be consistent not only with the aforementioned statistical results but also with additional analysis of TS pressure profiles, and in agreement with several theoretical models. As well, the emergence of turbulence self-organization in the edge might play a role in two measured effects: on the one hand, the generation of a subcritical pressure gradient might be a decisive factor for avoiding disruptive MHD modes, crucial for the achievement of high-β regimes. On the other hand, fully-developed self-organized dynamics could contribute to the degradation of heating efficiency and divergence from the ISS95 scaling, observed in the same $\langle\beta\rangle$ regimes. Regardless of its origin, the emergence of superdiffusive transport could eventually become a relevant obstacle for the realization of higher $\langle\beta\rangle$ and further study should be addressed. In this sense, the present work could be advanced by carrying out experiments with diagnostics capable of directly measuring fluctuations and radial transport in the edge with enough time resolution to repeat the presented tests (e.g. HIBP, Langmuir probes, etc.) and estimate the magnitude of self-similar transport. The results in this paper provide an example of the dependence of the nature of transport on a macroscopic control parameter such as $\langle\beta\rangle$. A closer analysis of such interplay could eventually prove valuable to increase LHD performance, and by extension, to reach an

efficient nuclear fusion reactor.

Acknowledgments

This work was partially supported by grant ENE2009-07247, Ministerio de Ciencia e Innovación, Spain and by NIFS/NINS under the project of Formation of International Network for Scientific Collaborations.

References

[1] M. Wakatani, *Stellarator and Heliotron Devices* (Oxford University Press, Oxford, 1998).
[2] S. Sakakibara et al., Plasma Phys. Control. Fusion **50**, 124014 (2008).
[3] A. Weller et al., Nucl. Fusion **49**, 065016 (2009).
[4] A. Komori et al., Phys. Plasmas **12**, 056122 (2005).
[5] K. Ichiguchi et al., Nucl. Fusion **43**, 1101 (2003).
[6] K.Y. Watanabe et al., Nucl. Fusion **45**, 1247 (2005).
[7] H. Funaba et al., Fusion Sci. Technol. **51**, 129 (2007).
[8] D. Carralero et al., Cont. Plasma Phys. 51, 92-98 (2011).
[9] D. del-Castillo-Negrete, Phys. Rev. Lett. **94**, 065003 (2005).
[10] B. Ph. van Milligen et al., Phys. Plasmas **11**, 2272 (2004).
[11] G. Dif-Pradalier et al., Phys. Rev. E **82**, 02541 (2010).
[12] H. E. Hurst, Trans. Am. Soc. Civil Eng. **116**, 770 (1951).
[13] R. Woodard et al., Physica A **373**, 215 (2007).
[14] B.A. Carreras et al., Phys. Plasmas **5**, 3632 (1998).
[15] B. D. Dudson et al., Plasma Phys. Control. Fusion **47**, 885 (2005).
[16] Y. H. Xu et al., Phys. Plasmas **11**, 5413 (2004).
[17] R. Sánchez et al., Phys. Rev. Lett. **90**, 185005 (2003).
[18] P. Bak et al., Phys. Rev. Lett. **59**, 381 (1987).
[19] H. J. Jensen, *Self-Organized Criticality* (Cambridge University Press, Cambridge, 1998).
[20] R.O. Dendy et al., Plasma Phys. Control. Fusion **49**, A95 (2007).
[21] D.E. Newman et al., Phys. Rev. Lett. **3**, 1858 (1996).
[22] S.C. Chapman et al., Phys. Plasmas **86**, 13 (2001).
[23] B.A. Carreras et al., Phys. Plasmas **3**, 2903 (1996).
[24] O. Motojima et al., Nucl. Fusion **47**, S668 (2007).